A Journal of the Gesellschaft Deutscher Chemiker

Angewandte International Edition GDCh Chemie

www.angewandte.org

Accepted Article

Title: Structural and Functional Characterization of an Amidase Targeting a Polyurethane for Sustainable Recycling

Authors: Laura Rotilio, Thomas Bayer, Hannes Meinert, Luis M. C. Teixeira, Martin B. Johansen, Andreas Sommerfeldt, Allan R. Petersen, Alexander Sandahl, Malene B. Keller, Jesper Holck, Pedro Paiva, Daniel E. Otzen, Uwe T. Bornscheuer, Ren Wei, Pedro A. Fernandes, Maria J. Ramos, Peter Westh, and Jens Preben Morth

To be cited as: *Angew. Chem. Int. Ed.* **2024**, e202419535

Link to VoR: https://doi.org/10.1002/anie.202419535

WILEY VCH

10.1002/anie.202419535

WILEY VCH

RESEARCH ARTICLE

Structural and Functional Characterization of an Amidase Targeting a Polyurethane for Sustainable Recycling

Laura Rotilio[a][b], Thomas Bayer[c], Hannes Meinert[c], Luis M. C. Teixeira[a][d], Martin B. Johansen[a][e], Andreas Sommerfeldt[a][e], Allan R. Petersen[a][e], Alexander Sandahl[a][e], Malene B. Keller[b], Jesper Holck[b], Pedro Paiva[a][d], Daniel E. Otzen[a][f], Uwe T. Bornscheuer[c], Ren Wei[c], Pedro A. Fernandes[a][d], Maria J. Ramos[a][d], Peter Westh[a][b]*, J. Preben Morth[a][b]*

[a] Dr. L. Rotilio, MSc L. M. C. Teixeira, Dr. M. B. Johansen, Dr. A. Sommerfeldt, Dr. A. R. Petersen, Dr. A. Sandahl, Dr. P. Paiva, Prof. Dr. D. E. Otzen, Prof. Dr. P. A. Fernandes, Prof. Dr. M. J. Ramos, Prof. Dr. P. Westh and Prof. Dr. J. P. Morth
EnZync Center for Enzymatic Deconstruction of Thermoset Plastics
E-mail: petwe@dtu.dk; premo@dtu.dk.

[b] Dr. L. Rotilio, Dr. M.B. Keller, Dr. J. Holck, Prof. Dr. P. Westh and Prof. Dr. J. P. Morth
Biotechnology and Biomedicine
Technical University of Denmark
Søltofts Plads, DK-2800, Kongens Lyngby, Denmark.

[c] Dr. T. Bayer, MSc H. Meinert, Prof. Dr. U. T. Bornscheuer, Dr. R. Wei
Department of Biotechnology & Enzyme Catalysis
Institute of Biochemistry, University of Greifswald
Felix-Hausdorff-Str. 4, 17487 Greifswald, Germany

[d] MSc L. M. C. Teixeira, Dr. P. Paiva, Prof. Dr. P. A. Fernandes, Prof. Dr. M. J. Ramos
LAQV, REQUIMTE, Departamento de Química e Bioquímica
Faculdade de Ciências, Universidade do Porto
Rua do Campo Alegre s/n, 4169-007 Porto, Portugal

[e] Dr. M. B. Johansen, Dr. A. Sommerfeldt, Dr. A. R. Petersen, Dr. A. Sandahl
Danish Technological Institute
Kongsvang Alle 29, 8000 Aarhus, Denmark.

[f] Prof. Dr. D. E. Otzen
Interdisciplinary Nanoscience Center (iNANO).
Aarhus University
Gustav Wieds Vej 14, 8000 Aarhus, Denmark

Supporting information for this article is given via a link at the end of the document.

Abstract: Global plastic production exceeded 400 million tons in 2022, urgently demanding improved waste management and recycling strategies for a circular plastic economy. While the enzymatic hydrolysis of polyethylene terephthalate (PET) has become feasible on industrial scales, efficient enzymes targeting other hydrolyzable plastic types, such as polyurethanes (PURs), are lacking. Recently, enzymes of the amidase signature (AS) family, capable of cleaving urethane bonds in a polyether-PUR analog and a linear polyester-PUR, have been identified. Herein, we present high-resolution crystal structures of the AS enzyme UMG-SP3 in three states: ligand-free, bound with a suicidal inhibitor mimicking the transition state, and bound with a monomeric PUR degradation product. Besides revealing the conserved core and catalytic triad akin to other AS family members, the UMG-SP3 structures show remarkable flexibility of loop regions. Particularly, Arg209 in loop 3 adopts two induced-fit conformations upon ligand binding. Through structure-guided kinetic studies and enzyme engineering, we mapped structural key elements that determine the enhanced hydrolysis of urethane and amide bonds in various small molecules, including a linear PUR fragment analog. Our findings contribute critical insights into urethanase activity, aiding PUR degradation campaigns and sustainable plastic recycling efforts in the future.

Introduction

Global production of (synthetic) polymers approaches 400 Mt annually.[1] While plastics provide countless benefits for consumer products, the associated waste problems remain largely unsolved.[2] This has led to the consensus that a circular plastic economy is mandatory for future use.[3] Today, only 9% of all plastics ever made have been recycled.[4] More efficient recycling strategies are urgently needed to improve this shortcoming rapidly.[5] This has spurred intense research interest in different types of (synthetic) polymers, as well as their depolymerization to recover and recycle monomeric building blocks. In this regard, enzymatic bioprocessing of plastic waste has emerged as an auspicious approach.[6][7][8] Biocatalytic approaches can be initiated by pretreatment of the raw materials, followed by an enzymatic hydrolysis step to free the monomers. This strategy has proven very effective for the polyester polyethylene

10.1002/anie.202419535

terephthalate (PET), which is currently on the verge of full-scale industrial implementation.[9][10] Consequently, the enzymatic breakdown of other hydrolyzable plastics, such as polylactic acid (PLA), polyamides (PAs), and polyurethanes (PURs), is of great interest. Currently, PUR recycling processes involve chemical steps, leading to the recovery of constituent polymer building blocks.[11][12] While established strategies like mechanical recycling or chemical glycolysis are economically more feasible, (bio)chemical depolymerization yields monomeric building blocks that can be directly used for the manufacturing of virgin polymers (closed-loop recycling) or other value-added products (open-loop recycling).[8][10][13] In recent years, numerous examples of microbial degradation of PURs under mild and environmentally benign conditions have been reported. While the majority of studies focused on polyester hydrolases, only a few cases featured urethane-hydrolyzing enzymes.[14] Promising studies for a potential adaption for polymer recycling employed extracts from fungi and bacteria, the latter being often isolated from PUR-contaminated sites.[15] Many hydrolases, applicable for biodegradation, act on the ester bonds in the polyol constituents (i.e., the soft segments) of polyester-PUR structures.[16][17] However, these enzymes are inactive on the hard and recalcitrant segments in PUR materials containing the urethane (or carbamate) bonds.[14c][18] In 2023, Branson et al. discovered the first enzymes (UMG-SP1, UMG-SP2, and UMG-SP3) that effectively degraded the urethane bond in a toluene diisocyanate (TDI)-based polyether-PUR fragment, releasing the monomers diethylene glycol and 2,4- and 2,6-diaminotoluene.[19] The study was extended in 2024 with the release of the UMG-SP1 (hereafter referred to as SP1) crystal structure and mutants with enhanced hydrolytic activity; the previously reported crystal structure of SP1 was ligand-free and was suffering from disorder in the loop regions around the active site and thus does not provide direct insight into the product bound state.[20] These discoveries prompted us to elucidate the structure of the 4,4'-methylene diphenyl diisocyanate (MDI)-based polyester-PUR degrading urethanase UMG-SP3 (hereafter called SP3) (Scheme 1).[19] The sequence identity between SP3 and SP1 is 49%, while it is 80% with SP2. SP3 thus represent a more distant homologue to SP1, which contributes strongly to the structural diversity, critical for understanding and optimizing the kinetic and hydrolytic properties needed for PUR degradation. Based on high-resolution crystal structures of SP3 in ligand-free and ligand-bound states, we identified regions that are crucial for the hydrolysis of PUR fragments and demonstrated how rationally designed amino acid substitutions in these regions can lead to significant improvements in the enzymatic hydrolysis of urethane and amide bonds.

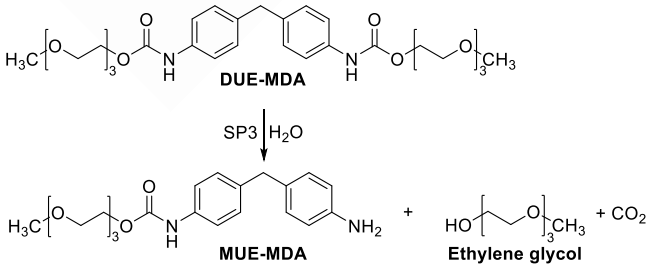

Scheme 1. Hydrolysis reaction mediated by SP3. Cleavage of di-urethane ethylene methylenedianiline (DUE-MDA) yields the asymmetric monosubstituted MUE-MDA, the ethylene glycol substituent, and carbon dioxide.

Results and Discussion

Architecture and Structural Features of SP3

The crystal structures of ligand-free SP3, PMS-bound SP3 (SP3:PMS), and 4,4'-MDA-bound SP3 (SP3:MDA) were determined at 2.32 Å, 2.18 Å, and 2.00 Å resolution, respectively as shown in the Supporting Information (SI; Table S1). Two polypeptide chains are present in the asymmetric unit, while the enzyme acts as a monomer in solution, as determined by size-exclusion chromatography (Fig. S1). The overall structure is composed of twelve α-helices (αA–L) surrounding ten core β-strands (β1–10), completing a fold common to hydrolytic enzymes, which usually is formed by twelve helices and eleven strands.[22][23]

The edges of the catalytic pocket are shaped by α-helices I (amino acid residues 293–308) and K (382–393), and the loops 1–4 (residues comprising L1: 76–103, L2: 119–153, L3:189–214, and L4: 351-382; Fig. 1a). The active site is located within a cavity, centrally positioned in an elongated cleft, which is highly solvent exposed and extends over 25 Å. The Lys76 in proximity to the amidase signature sequence motif (G149–G154: GGSSGG) establishes contacts with surrounding residues *cis*Ser151, Ser152, Ser170, and Ser175 (Fig. 1b).[24] We identified Ser175-*cis*Ser151-Lys76 as the catalytic triad responsible for amide hydrolysis, a conserved feature among the AS family.[25][26] The reaction is likely initiated by Ser175, which acts as the primary nucleophile being positioned for attack on the substrate and forming the tetrahedral intermediate, which is stabilized by the oxyanion hole. The latter is comprised of the residues Ile172 and Gly173 in SP3. The bridging residues *cis*Ser151 and Lys76 assist the enzymatic catalysis by respectively shuttling protons (between Ser175 and Lys76), with Lys76 likely acting as the general acid/base.[19][27][28] The unusual *cis* conformation of Ser151 is maintained by a strong hydrogen bond network between the triad and is reinforced by the presence of Ser152 and Ser170 (Fig. 1b).

The crystal structure of SP3 superposes with crystallographic structures of SP1 (PDB 8S7Z) and SP2 (PDB 8WDW), with a root mean square deviation (RMSd) of 0.77 Å (over 401 Cα atoms) and 0.39 Å (over 434 Cα atoms), respectively, showing an identical overall architecture that is also reflected in the same hydrogen bonding network around the catalytic triad.[20][21] The comparison also highlights the conservation of L1–4 surrounding the active site (SI, Fig. S2a–b), with L3 having the highest degree of movement.

The closest structural homologs identified using the Dali server are a fatty acid amide hydrolase (FAAH) from *Candida albicans* (*Ca*FAAH; PDB 6KVR) and ClbL (PDB 8ES6), an amidase from colibactin gene cluster of certain *E. coli* species.[29][30][31] *Ca*FAAH and ClbL share 25% and 33% sequence identity to SP3, respectively. Both superpose with an RMSd of 1.8 Å covering 405 Cα atoms. FAAHs are well-characterized members of the AS family involved in the catabolism of fatty acid amide molecules

10.1002/anie.202419535

RESEARCH ARTICLE

and part of the endocannabinoid system, thus making FAAHs interesting targets for drug development.[32][33] The amidase ClbL is involved in the last step of the colibactin synthetic pathway as part of a larger molecular complex.[31] The overall fold is virtually identical between SP3 and ClbL, whereas additional helical domains are present in *Ca*FAAH, distinguishing it from the SP3 architecture. However, the quintessential core domain of AS members (SI, Fig. S2c) – the residues responsible for hydrolytic activity and L1–4 – are highly conserved features among all structures (SI, Fig. S2d). As in SP3, the substrate binding pocket of *Ca*FAAH and ClbL is hydrophobic and exposed to the surface. These results highlight the functional importance of the distinctive structural features in amidases, alongside the presence of flexible elements surrounding the active site, which might contribute to the wide range of substrates hydrolyzed by AS family members.[34] Nonetheless, the biological function of SP3 – and the other two metagenomic homologs – remains unclear.

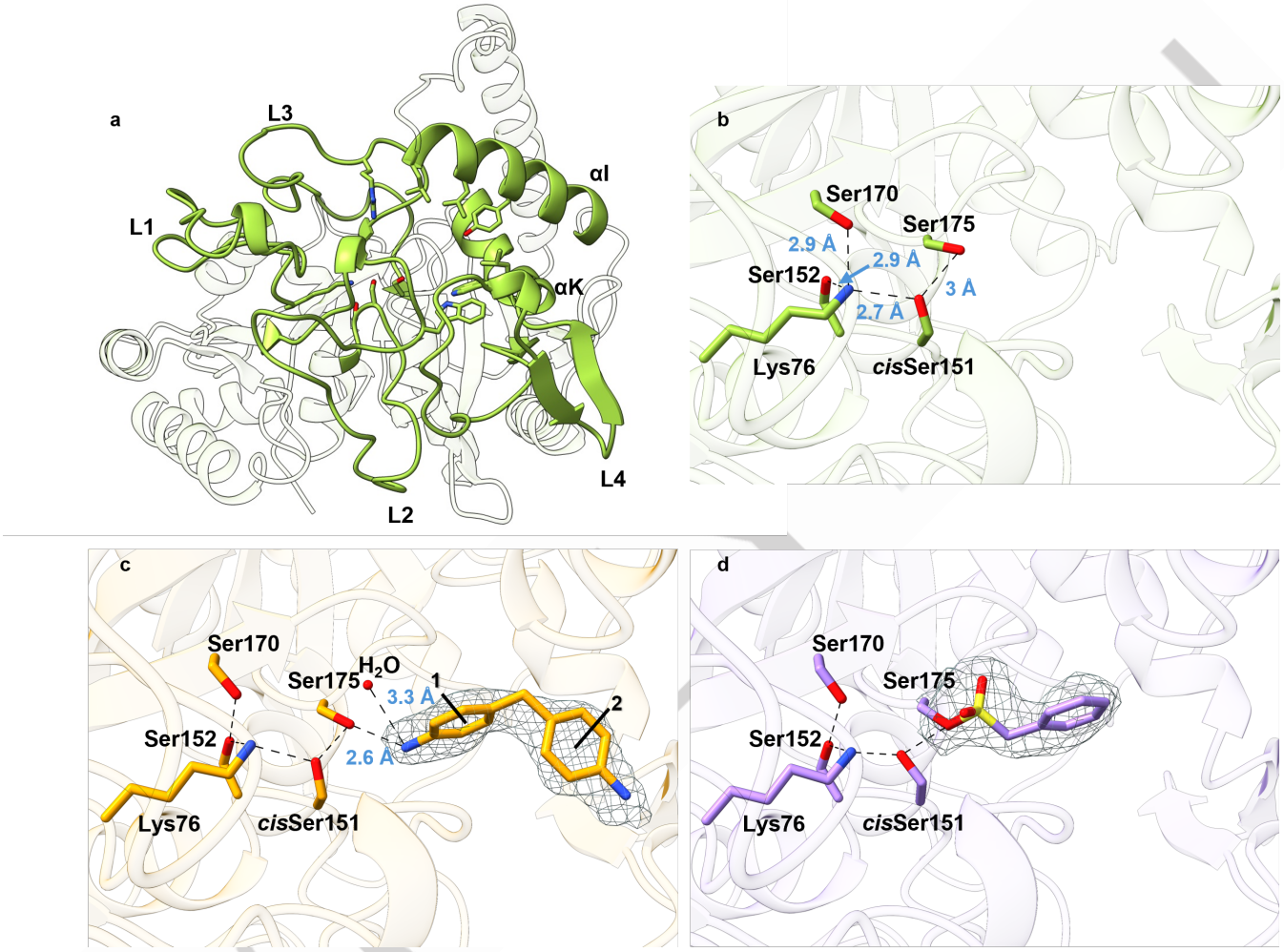

Figure 1. Crystal structures of SP3. a) SP3 overall monomeric arrangement. The edges of the catalytic pocket (in green) correspond to α-helices I (293–308) and K (382–393) and L1–4 (residues L1: 76–103; L2: 119–153; L3: 189–214; L4: 351-382). b) Close-up of the catalytic triad (Ser175-*cis*S151-Lys76), interacting (dashed lines) with surrounding residues Ser170 and Ser152. c) SP3 in complex with 4,4'-MDA (aniline moieties are numbered 1 and 2), interacting with Ser175 and a water molecule. 2mFo-Fc omit map at 4σ is shown. Hydrogen bond interactions are represented with dashed lines. d) SP3 in complex with phenylmethanesulfonic acid (PMS) covalently bound to Ser175. 2mFo-Fc omit map at 4 σ is shown. Hydrogen bond interactions represented with dashed lines, bond length colored in cyan.

SP3 in Complex with 4,4'-MDA and PMS

The primary objective of the structural analysis was to elucidate the interactions of SP3 with a PUR analog, thereby establishing the molecular basis for substrate binding and product release to guide enzyme engineering. Soaking attempts using pure product analog 4,4'-MDA were unsuccessful and detrimental to crystal quality. Instead, we synthesized a more soluble substrate analog that constituted a fraction analog of a typical polyether-PUR, herein referred to as di-urethane ethylene methylenedianiline (DUE-MDA); the chemical structure is shown in Scheme 1. Gratifyingly, extensive soaking attempts on SP3 crystals with DUE-MDA allowed us to identify electron density that could be built as 4,4'-MDA. This means that *in crystallo,* catalysis must have taken place. The modeled 4,4'-MDA molecule approximates the typical bond angle of the sp^3 hybridized methylene bridge (here 114° compared to the optimal angle of 109.5°) connecting

10.1002/anie.202419535

the two aniline groups (Figure 1c). The amine group of the aniline moiety 1 is hydrogen bonded to the catalytic Ser175 and a water molecule (Fig. 1c). The molecule sits in the first portion of the substrate binding pocket encapsulated in a hydrophobic region with each aniline ring (1 and 2) engaged in strong π-π interactions with Trp128 and Trp367, respectively (SI, Fig. S3a). in SP1 and SP2, Trp128 is conserved, while the position equivalent to Trp367 is only conserved in SP2. In SP1, this residue position has been deleted from the sequence and the loop region in the crystals structure of SP1 (PDB ID 8S7Z) is disordered, precluding structural comparison. In addition, we determined a crystal structure with well-defined electron density attributed to the phenylmethylsulfonate (PMS) ester formed with the catalytic Ser175. Phenylmethylsulfonyl fluoride (PMSF) is commonly used in protein purification as a mechanism-based inhibitor of serine proteases and related hydrolases. PMSF reacts and forms a covalent bond with Ser175 (Fig. 1d) and provides a valuable tool for mimicking the tetrahedral intermediate formed during catalysis. This covalent adduct has also been observed in the ClbL structure.[31] In the SP3 crystal structure, the sulfonyl group interacts with the oxyanion hole (Ile172 and Gly173) and protein backbone, while the benzylic ring is in hydrophobic contacts with Trp128, Ile172, and Leu385 with average interaction distances of 3.7–4.0 Å (SI, Fig. S3b).

When comparing the ligand-free and the SP3:MDA structures, the overall enzyme architecture is retained with minimal shifts detected in the side chains that surround the catalytic pocket. The most striking difference involves Arg209 (located in L3), which adopts an inward and outward conformation, respectively, in unbound and 4,4'-MDA-bound structures (Fig. 2a). This plasticity allows the Arg209 side chain to shift position upon ligand binding from close to the active site to being turned out from the active site, resulting in a 180° flip of the residues 207–211 in L3 and the relocation of Arg209 by 17 Å. When Arg209 is in the inward arrangement, the guanidinium group engages with Trp88 through a cation-π interaction. In contrast, the outward arrangement is structurally stabilized by a constellation of hydrogen bonds and salt bridges with nearby residues Glu193 and Glu211. Comparing the 4,4'-MDA- and PMS-complexed structures, we noticed that L3 adopts an equivalent conformation (Fig. 2b). Moreover, the aromatic aniline moiety 1 of 4,4'-MDA superposes with the benzylic ring of PMS (Fig. 2b), suggesting the likely position that DUE-MDA and possibly longer PURs adopt during catalysis. With these structures in complex with ligands resembling a PUR fragment, we provide the first mapping of SP3 critical features related to its catalytic properties, as discussed in the next section.

Computational studies on SP3 structures

To assess the stability of the structural features observed in the crystallographic structures, we simulated the unbound SP3, the PMS-bound SP3, and the 4,4'-MDA bound SP3 structures. In the absence of any ligand, Arg209 was facing the active site and was inserted into a hydrophobic pocket (SI, Fig. S4a). We observed that the system was stable and that this feature was maintained throughout the entire simulation (Fig. 3a–b). During the simulation, Arg209 established several hydrogen bonds with nearby water molecules and with the backbone of residues, such as Ala124, Val307, Leu308, and Gln310. These interactions contribute to the stabilization of Arg209. Additionally, the presence of bulky residues within the hydrophobic pocket, such as Trp88 and His200, likely reduces the freedom of movement for Arg209, further stabilizing this residue within the cavity. On the other hand, when a ligand was bound to the enzyme, Arg209 reoriented to face the solvent side. Throughout our simulation, this reorientation facilitated several stabilizing electrostatic interactions with Asp193, Glu198, and Glu211, as well as π-cation interactions with Tyr201 and Trp325 (SI, Fig. S4b). Arg209 also established hydrogen interactions with the solvent. Compared to the unbound structure, both Arg209 and L3 exhibited increased mobility and flexibility. Nevertheless, the outward arrangement of Arg209 was consistently maintained throughout the entire simulation (Fig. 3b).

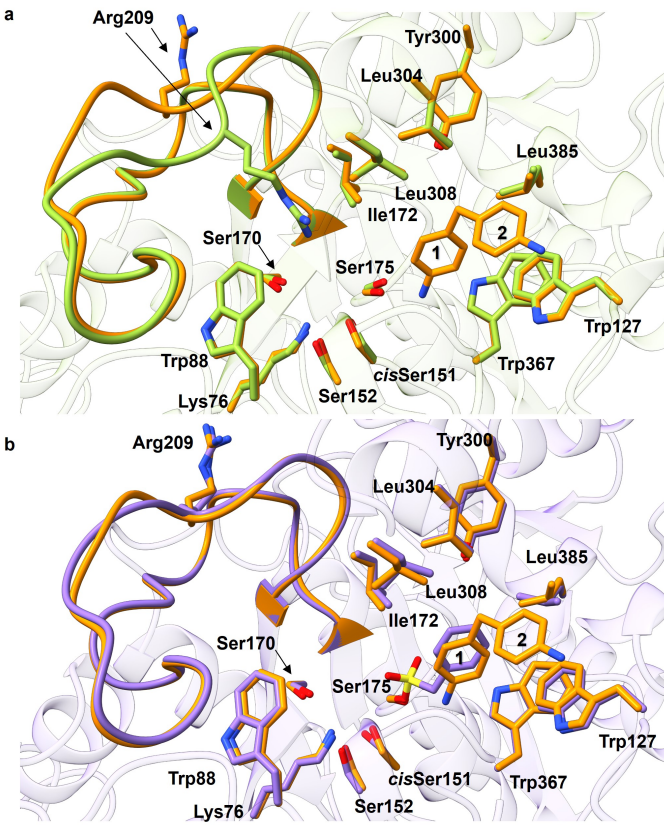

Figure 2. Analysis of SP3 structures. a) Superposition between unbound (green) and MDA-bound (orange) SP3 structures showing the different arrangements of Arg209 upon ligand binding. The catalytic triad is Ser175-*cis*Ser151-Lys76; residues Ser170, Ser152, Ile172, Leu308, Leu304, Tyr300, Leu385, Trp88, Trp367, and Trp127 form the active site cavity. b) Superposition between MDA-bound (orange, aniline moieties are numbered 1 and 2) and PMS-bound (purple) SP3 structures showing an identical conformation in the active site.

10.1002/anie.202419535

Interestingly, when we transferred PMS to the unbound SP3 crystal structure (here designated by altered MD), we observed that Arg209 transitioned to the outward arrangement during half of the simulation (SI, Fig. S4c and Fig. 3b). Accordingly, we observed an increase in the flexibility and mobility of Arg209 and L3 compared to the unbound SP3 structure, demonstrating the role of ligand binding in positioning Arg209. In line with the PMS-bound structure, the Arg209 outward arrangement was stabilized through the establishment of electrostatic interactions with Asp193, Glu198, and Glu211, π-cation interactions with Tyr201 and Trp325, and hydrogen interactions with solvent molecules. Concerning the 4,4'-MDA system, we observed that the hydrophobic pocket in which the ligand was inserted played a vital role in its stabilization. The π-π interactions exhibited in the crystallographic structure aided in the stabilization of 4,4'-MDA within the pocket (Fig. S4d) and favored the ligand to remain positioned throughout most of the simulation (Fig. 3c).

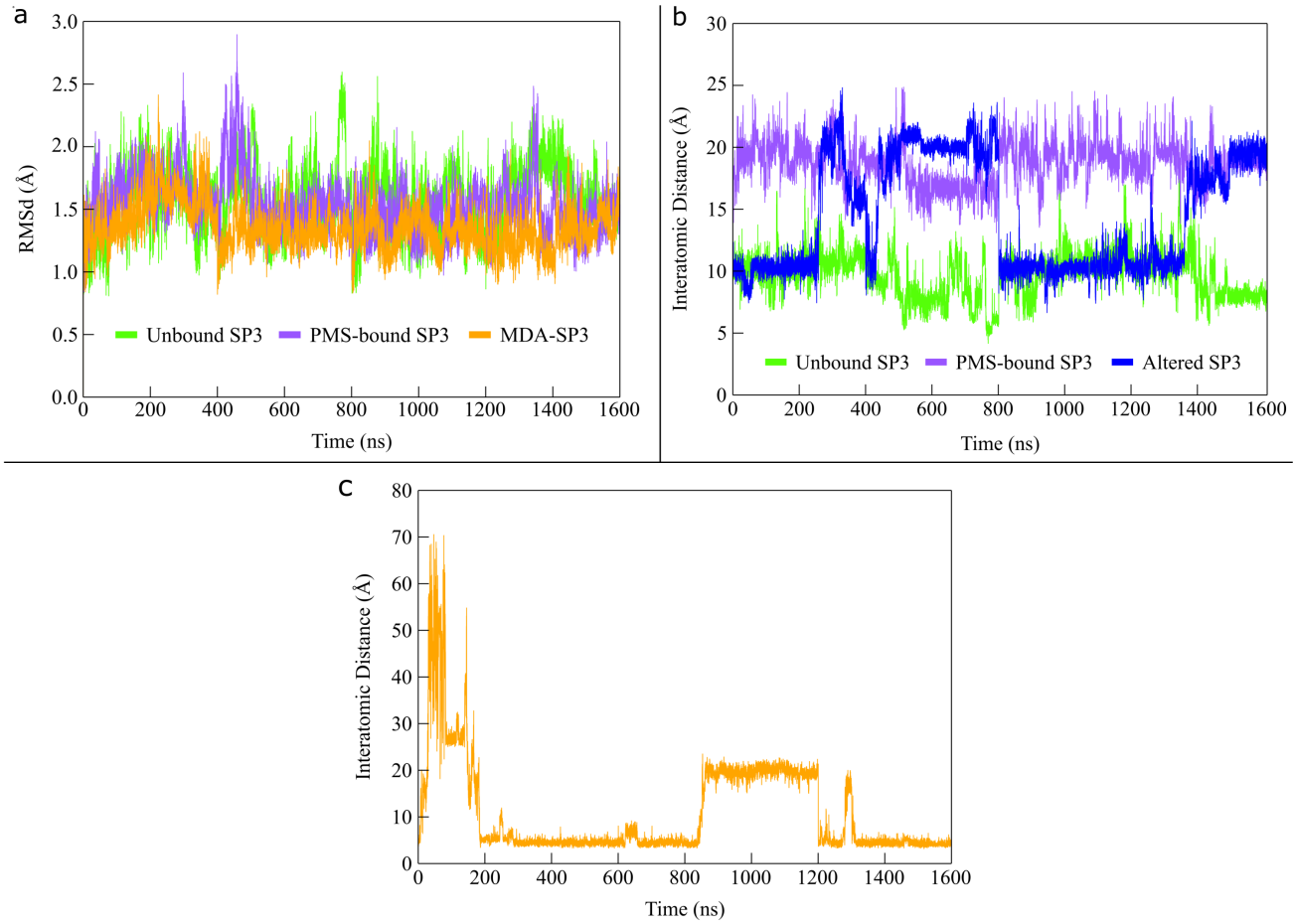

Figure 3. Stability assessment by MD simulations. a) Graphical representation of the RMSd evolution throughout the MD simulations of the unbound structure (green), SP3:PMS (purple), and SP3:MDA (orange). b) Graphical representation of the distance of Arg209 to the active site (given by the distance of Arg209 Cζ to the Ser151 Oγ) for the unbound structure, the SP3:PMS, and the altered MD structure (blue). c) Graphical representation of the distance between 4,4'-MDA to the hydrophobic pocket (given by the distance between 4,4'-MDA and the Trp367).

Enzymatic Characterization on Di-Urethane Ethylene Methylendianiline (DUE-MDA)

To determine urethanase activity towards PUR, we synthesized a substrate analog that mimics a fraction of a typical polyether-PUR, DUE-MDA (Scheme 1, see also SI Fig. S5). This substrate was converted readily by all three wild-type enzymes (SP1, SP2, and SP3), and we used LC-MS to monitor the reaction progress. As illustrated in the SI, the dominant reaction was the cleavage of one urethane bond and the associated release of a diethylene glycol methyl ether substituent and a monosubstituted MDA-urethane, henceforth referred to as MUE-MDA (Scheme 1, see also SI Figs. S6 and S7). The latter compound was a poor substrate. Hence, we only found deficient concentrations of (unsubstituted) 4,4´-MDA in the hydrolysates (SI, Figs. S8 and S9). Based on our findings, we propose the hydrolytic reaction with DUE-MDA, as shown in Scheme 1. Initial activity measurements for DUE-MDA with different incubation times showed linear progress curves for about 1 h, and we subsequently used 30 min samples for steady-state kinetic analyses. Results in Fig. 4a show initial rates (circle) and best fits of the Michaelis-Menten equation (lines). The kinetic parameters derived from this data are listed in Table 1. The maximal turnover on the DUE-MDA substrate is in the 1–2 s^{-1} range, with Michaelis constants in the high micromolar range for all three enzymes and,

10.1002/anie.202419535

as a result, specificity constants in the range of 1–4 x 10^3 $M^{-1}s^{-1}$ (Table 1).

Table 1. Steady-state kinetic parameters on DUE-MDA.[a]

	SP1	SP2	SP3
k_{cat} (s^{-1})	2.4 ± 0.20	0.9 ± 0.04	1.8 ± 0.04
Km (μM)	590 ± 17	760 ± 80	490 ± 29
k_{cat} /Km (s^{-1}/M^{-1})	4.10 x 10^3	1.16 x 10^3	3.63 x 10^3

[a] Mean and standard deviation from two independent measurements.

Activity against DUE-MDA was also studied in endpoint measurements after 24 h. While SP1 and SP2 had comparable performance, yielding ~0.3 mM of MUE-MDA (Fig. 4b). In general, the results obtained in these prolonged experiments suggested much lower performance than predicted from the steady state kinetic parameters in Tab. 1, and this could be related to product precipitation or enzyme instability. The effect was particularly strong for SP3, which was approximately 3-fold less active compared to SP1 and SP2 (Fig. 4b), and this could reflect the lower thermal stability of SP3 [19], a point that future engineering efforts should prioritize.

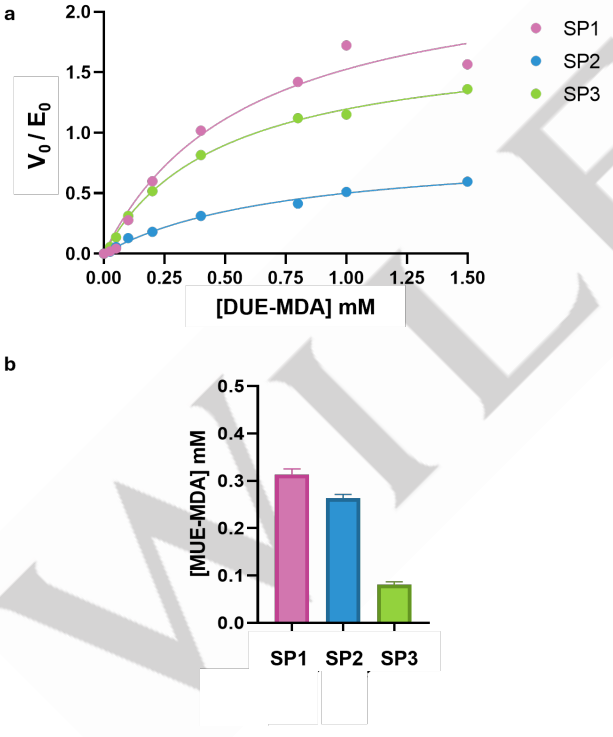

Figure 4. Biochemical characterization on DUE-MDA. a) Michaelis-Menten curves of SP1, SP2, and SP3 obtained from monitoring DUE-MDA hydrolysis. b) MUE-MDA production within 24 h. Reaction conditions as follows: 0.1 μM enzyme, 2.0 mM DUE-MDA trimer (5% (v/v) solvent in the reaction mixture) in 50 mM HEPES, 100 mM NaCl (pH 7.5) at 25 °C with shaking (300 rpm). Bars represent the mean and standard deviation (SD) from two independent measurements.

In Silico Analysis of Engineering Variants of SP3

As L3 is expected to be responsible for substrate recognition, we targeted four L3 residues (Arg204, Arg209, Gly210, and Glu211) to assess their impact on the structural features of SP3.[20] Regarding the substitutions of Arg204 (R204A and R204G), we observe that in both cases, L3 had a significant increase in mobility and flexibility (SI, Fig. S10a). In the ligand-free wild-type SP3, Arg204 established a hydrogen bond with His93 and a strong electrostatic interaction with Asp95 (SI, Fig. S10b). Both substitutions resulted in the loss of these stabilizing interactions. Based on the striking difference in the arrangement of Arg209 in the absence and presence of ligands, substitutions to a hydrophobic residue (loss of charge) or a negatively charged residue (charge inversion) were of interest to understand the impact of this residue in L3. As discussed above, in the absence of a ligand, Arg209 exhibited a stable inward arrangement. Consequently, unlike the wild-type, the residue was not fully inserted into the pocket, increasing its freedom of movement (SI, Fig. S10b). This increase in freedom of movement due to the size reduction was also observed in the R209E substitution, ultimately resulting in a less stable inward arrangement. On the other hand, in the presence of a ligand, wild-type Arg209 presented an outward arrangement that allowed for the establishment of stable electrostatic and π-cation interactions. For the R209A substitution, the charge was lost, meaning Ala209 could not establish the interactions necessary for stabilization. For the R209E substitution, the positive charge was replaced by a negative charge. Given that the vicinity of the outward arrangement of this residue contained several negatively charged residues (SI, Fig. S4b), we conclude that the introduction of this negative charge promoted electronic repulsion. Additionally, the replacement of the positive charge abolished the π-cation interactions. Consequently, once again, the outward arrangement was not stabilized. Thus, both substitutions destabilized L3 by eliminating the stabilizing interactions of Arg209 in both possible arrangements. We observed that both Gly210 substitutions (G210A and G210T) led to an increase in the flexibility and mobility of L3 (SI, Fig. S10a). That is, both substitutions resulted in a less stable residue, which in turn reduced the stability of L3, making it more mobile. In contrast, E211P led to a decrease in the flexibility and mobility of L3 (SI, Fig. S10a). Inspection of wild-type ligand-free SP3 revealed that, despite establishing some hydrogen interactions with nearby residues (e.g., Leu212 and Gln332) and water molecules, Glu211 was surrounded by several hydrophobic residues (e.g., Leu212, Val307, Trp325, and Leu329). This meant that its negative charge was not favorable for its hydrophobic surrounding (SI, Fig. S10b). Indeed, when Glu211 was substituted for a proline, we observed a reduction in the mobility of this residue, promoted by hydrophobic interactions with its surrounding residues. Consequently, the stabilizing effect of E211P reduced the flexibility and mobility of L3. In contrast, the E211A substitution did not produce the same effect. Despite Glu211 also being substituted to a hydrophobic residue, this substitution led to an increase in the flexibility and mobility of L3. All substitutions promoted an increase in the mobility of L3, except for the E211P substitution, which is consistent with the general

10.1002/anie.202419535

increase in rigidity associated with the introduction of Pro residues, ultimately, leaving more avenues open for future bioengineering.

Experimental Verification of Engineered Variants of SP3

We reasoned that a more flexible (i.e., easily activated) SP3 might exhibit greater hydrolytic properties. To test this hypothesis, we targeted the equivalent residues in L3 (Fig. 5a) by site-directed mutagenesis: Arg204, Arg209, Gly210, and Glu211 (Fig. 5b). Substitutions included conservative amino acid exchanges (e.g., R204K, R209K, and E211D), different spatial requirements (e.g., R204G, R209A), and the introduction of opposite charges (e.g., R209E). Subsequently, apparent specific activities were determined against the small carbamates 7-carbethoxyamino-4-methylcoumarin (CAMC, Fig. 5c) and ethyl *N*-nitrophenyl carbamate (ENPC, Fig. 5c) as described previously for the metagenomic urethanase SP1.[20] Compared to SP1 (CAMC: 798 ± 193 mU mg^{-1}; ENPC: 14 ± 5 mU mg^{-1}), SP3 exhibited similar apparent specific activities of 597 ± 178 mU mg^{-1} and 18 ± 8 mU mg^{-1} for CAMC and ENPC, respectively.[20] The specific activity of SP3 for CAMC also agrees with an earlier study.[19] While conservative amino acid exchanges at position Arg204 (R204K and R204H), as well as the introduction of a small, aliphatic alanine residue (R204A) yielded specific activities comparable to the wild-type enzyme (Table 2), the mutant R204G showed improved hydrolysis of CAMC (1,195 ± 180 mU mg^{-1}) and ENPC (40 ± 11 mU mg^{-1}).

Table 2. Specific activities of L3 variants of SP3.[a]

Mutant	CAMC	ENPC	CAMC Fold change	ENPC Fold change
WT [b]	597 ± 187	18 ± 8	-	-
R204A	387 ± 42	14 ± 6	0.60	0.77
R204G	1,195 ± 180	40 ± 11	2.00	2.22
R204H	473 ± 169	16 ± 4	0.80	0.90
R204K	862 ± 156	36 ± 10	1.44	2.00
D206N	1,009 ± 148	45 ± 15	1.70	2.50
G207S	703 ± 140	21 ± 12	1.17	1.16
R209A	620 ± 123	47 ± 20	1.03	2.60
R209H	473 ± 169	23 ± 12	0.80	1.27
R209K	472 ± 38	35 ± 14	0.80	1.94
R209N	352 ± 67	23 ± 10	0.60	1.27
R209Q	390 ± 48	35 ± 20	0.65	1.94
R209D	263 ± 78	5 ± 3	0.44	0.27
R209E	116 ± 24	2 ± 1	0.20	0.11
G210A	1,137 ± 260	34 ± 2	1.90	1.90
G210C	1,392 ± 364	34 ± 7	2.33	1.90
G210S	1,664 ± 272	34 ± 2	2.78	1.90
G210T	1,332 ± 219	38 ± 17	2.23	2.11
E211A	678 ± 54	42 ± 21	1.13	2.33
E211P	1,536 ± 203	59 ± 21	2.57	3.27
E211D	304 ± 79	10 ± 5	0.50	0.55
E211N	310 ± 13	29 ± 14	0.51	1.61
E211Q	499 ± 125	16 ± 10	0.83	0.88

[a] Specific activities [mU mg^{-1}] reported as mean values ± SD of biological replicates (n ≥ 3). [b] WT, wild-type SP3

Although various substitutions at position Arg209, which showed the largest displacement between free and ligand-bound structures of SP3 (Fig. 2a), reduced the activity towards CAMC, the hydrolysis of ENPC was significantly improved (Table 2). For example, the mutants R209Q and R209A exhibited close to 2- and 3-fold enhanced activity against ENPC, respectively. Similar to other residues, R209A was predicted to increase the flexibility of L3 *in silico* (SI, Fig. S10a). Noteworthy, the introduction of an opposite charge (R209E and R209D) strongly impaired the activity of SP3 against CAMC as well as ENPC (Table 2). The introduction of larger residues at position G210 significantly raised the hydrolytic activity of SP3 towards the small carbamates; exhibiting the highest increase (about 3-fold for CAMC and 4-fold for ENPC) observed amongst the investigated single amino acid exchanges in L3 (Table 2). Lastly, the substitutions E211P and E211A also produced more active enzyme variants with apparent specific activity increased to 1,536 ± 203 mU mg^{-1} for CAMC and 59 ± 21 mU mg^{-1} for ENPC with roughly 3-fold increase for both substrates. Noteworthy, a conservative exchange (E211D) or the removal of charged sidechains (E211Q and E211N) reduced the hydrolytic activity (Table 2). Interestingly, beneficial amino acid exchanges in L3 of SP3 naturally occur in the two other metagenomic urethanases, SP1 and SP2.[19][20] These include R204G (corresponding to Gly205 in SP1 and Arg204 in SP2) or E211P (Pro212 in SP1 and Asp211 in SP2). Improved mutants of SP3 also included G210A, G210C, G210S, and G210T; SP1 and SP2 feature a threonine and an alanine at the corresponding positions in L3 (Thr211 and Ala210, respectively). Consequently, we created two variants of SP3 – D206N and G207S, based on Asn207 and Ser207 found in SP1 and SP2, respectively – to reflect the natural diversity of amino acids in L3. Both variants hydrolyzed the two carbamates CAMC and ENPC more efficiently than the wild-type SP3 (Table 2). Together, these results confirm experimentally the importance of L3 for the hydrolytic activity of SP3; L3 and interacting amino acid residues – adjacent and distal – represent valuable mutational hotspots.

Conclusion

Recently, the enzymes SP1, SP2, and SP3 were shown to hydrolyze urethane bonds in PUR fragments, strongly motivating new research aiming at an in-depth understanding and characterization of AS family members.[19][20][21] Herein, we investigated the structural and biochemical features of SP3 based on three high-resolution crystal structures, one ligand-free and two in complex with ligands. These not only allowed us to confirm structural features shared by all three metagenomic urethanases

10.1002/anie.202419535

and related enzymes like the catalytic triad (Lys76, *cis*Ser151, and Ser175 in SP3) and four flexible loops (L1–4) that form the catalytic pocket.[20][21] We further report the first structure-based mapping of key residues in the active site pocket (Trp127, Ile172, Gly173, Trp367, Tyr300, Leu304, Leu308, Trp367, and Leu385) and the rearrangement of loops upon ligand binding as observed for L3 (Fig. 2a). The functional importance of L3 was also predicted by MD simulations and, ultimately, confirmed by different site-directed mutagenesis strategies targeting the residues in L3. Indeed, several of the 22 variants of SP3 showed up to a 3-fold improvement in specific activity over the wild-type enzyme against two model carbamates (CAMC and ENPC; Table 2). The increased activity followed the predicted flexibility increase of L3, except E211P, which was the only exchange predicted to lower the freedom of movement of L3 (Fig. S10c). Interestingly, while the transplantation of certain naturally occurring loop residues in SP1 and SP2 improved the activity of SP3 (e.g., D206N, G207S, or E211P), the substitution of Arg209 with acidic sidechains impaired catalysis significantly.The data suggest residue position 211 to be important for catalytic functionality, with enhanced flexibility being only one of many possibilities for increased catalytic activity. Side chains of prolines, aspartates, and glutamates are able to engage in π-π interaction[36] and might explain a contribution of this position in substrate recognition. However, further experimental work will be required to substantiate such hypotheses. This is in contrast to SP1, for example, featuring a glutamate residue at the corresponding position that is catalytically important. A detailed discussion of the underlying interactions and mechanisms will require thorough experimental engineering campaigns, for example, which is beyond the scope of the presented study and will be followed in the future. Towards the depolymerization of polymeric material, we compared the kinetic parameters of SP3 with SP1 and SP2, monitored for the hydrolysis of DUE-MDA and yielding specificity constants >10^3 M^{-1} s^{-1} (Table 1). These data highlighted that the major product was the monosubstituted MUE-MDA (Scheme 1); the completely hydrolyzed product, 4,4´-MDA, was only detected in trace amounts for all three enzymes. Endpoint measurements (Fig. 4b) showed SP3 to be inferior to SP1 and SP2. This deviates from steady-state kinetic parameters (Table 1) but might be explained by the poor thermostability of SP3, which becomes dominant during longer reaction times.[19] Together, these findings confirmed the importance of flexible loop regions in metagenomics urethanases and will assist the deeper understanding of structure-function relationships in AS family members.[20] In a wider perspective, bioprocessing of PUR is still in its infancy. We note, however, that the current status is reminiscent of early stages of work on PET hydrolases almost 20 years ago. This implies that the way forward includes enzyme discovery and engineering – with stability, specificity and catalytic efficiency as targets. The current results with wild-type specificity constants over 10^3 $M^{-1}s^{-1}$ on relevant PUR fragments and substantial activity improvements by structure guided point-mutations appear to bring some promise for progress along those lines.

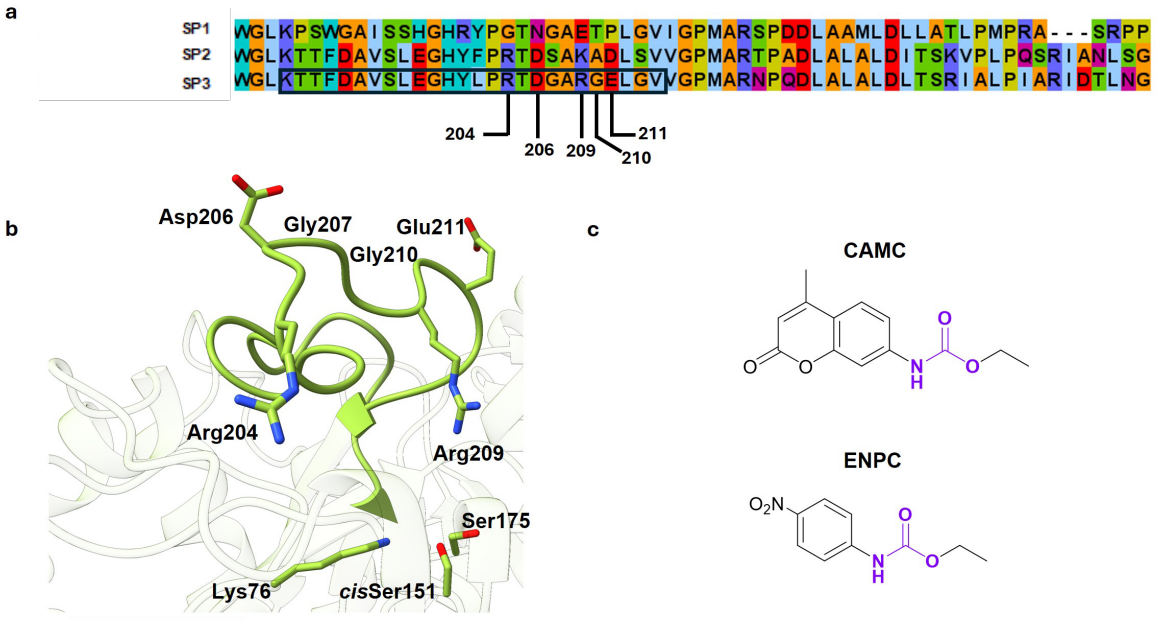

Figure 5. Engineered variants of SP3. a) Sequence alignment of SP1, SP2 and SP3 focusing on Loop 3 of SP3 (black rectangle). Numbers indicate the position chosen in the SP3 sequence for mutagenesis. b) Location of the mutated residues in L3 of SP3 with respect to the catalytic triad Ser175-*cis*S151-Lys76. Positions of Gly207 and Gly210 are indicated in the cartoon representation. c) Chemical structures of CAMC and ENPC used to screen the engineered variants.[20]

Supporting Information

The authors have cited additional references within the Supporting Information.[37-53]

Acknowledgments

EnZync is supported by Challenge grant NNF22OC0072891 from the Novo Nordisk Foundation. We are grateful to the rest of the EnZync consortium members for constructive and helpful feedback. LMCT, PP, PAF and MJR acknowledge the financial support of FCT/MCTES (LA/P/0008/2020 DOI 10.54499/LA/P/0008/2020, UIDP/50006/2020 DOI 10.54499/UIDP/50006/2020 and UIDB/50006/2020 DOI 10.54499/UIDB/50006/2020), through national funds. LMCT, PP, PAF, and MJR would further like to thank the European High-Performance Computing Joint Undertaking (EuroHPC JU) that granted access to MeluXina, the petascale EuroHPC supercomputer located in Bissen, Luxembourg, under proposal EHPC-REG2023R03-163. The synchrotron data was collected at the Biomax operated by MAXIV storage ring (MAXIV, Lund, Sweden), proposal number 20220405. We thank Ana Gonzalez for her help during data collection. We acknowledge DESY (Hamburg, Germany), a member of the Helmholtz Association HGF, for the provision of experimental facilities. Parts of this research were carried out at PETRAIII and we would like to thank Kirill Kovalev for his assistance. Beamtime was allocated for proposal MX992. Preliminary diffraction data was also collected at PETRAIII under proposal number MX992. We also acknowledge the European Synchrotron Radiation Facility (ESRF) for the provision of synchrotron radiation facilities under proposal number MX2604 and we would like to thank David Flot for assistance and support in using beamline ID30B under proposal number MX2604.

Keywords: amidase • crystal structure • enzyme catalysis • protein engineering • thermoset plastic

[1] Statista, “Global plastic production 1950-2022” can be found under https://www.statista.com/statistics/282732/global-production-of-plastics-since-1950/. (accessed: 30 September 2024)

[2] A. L. Andrady, M. A. Neal, *Philos. Trans. R. Soc. B* **2009**, 364, 1526, 1977-84.

[3] I. Vollmer, M. J. F. Jenks, M. C. P. Roelands, R. J. White, T. van Harmelen, P. de Wild, G. P. van der Laan, F. Meirer, J. T. F. Keurentjes, *Angew. Chem. Int. Ed.* **2020**, 59, 36, 15402-15423.

[4] N. Singh, T. R. Walker, *npj Mater. Sustain.* **2024**, 2, 17.

[5] N. Simon, K. Raubenheimer, N. Urho, S. Unger, D. Azoulay, T. Farrelly, J. Sousa, H. van Asselt, G. Carlini, C. Sekomo, M. L. Schulte, P. Busch, N. Wienrich, L. Weiand, *Sci.* **2021**, 373, 6550, 43-47.

[6] a) R. Wei, T. Tiso, J. Bertling, K. O’Connor, L. M. Blank, U. T. Bornscheuer, *Nat. Catal.*, **2020**, 3, 867-871; b) L. D. Ellis, N. A. Rorrer, K. P. Sullivan, M. Otto, J. E. McGeehan, Y. Román-Leshkov, N. Wierckx, G. T. Beckham, *Nat. Catal.* **2021**, 4, 539–556; c) V. Tournier, S. Duquesne, F. Guillamot, H. Cramail, D. Taton, A. Marty, I. André, *Chem. Rev.* ***2023***, 123, 9, 5612–5701.

[7] S. Kakadellis, G. Rosetto, *Sci.* **2021**, 373, 6550, 49-50.

[8] T. Uekert, A. Singh, J. S. DesVeaux, T. Ghosh, A. Bhatt, G. Yadav, S. Afzal, J. Walzberg, K. M. Knauer, S. R. Nicholson, G. T. Beckham, A. C. Carpenter, *ACS Sustainable Chem. Eng.* **2023**, 11, 3, 965–978.

[9] V. Tournier, C. M. Topham, A. Gilles, B. David, C. Folgoas, E. Moya-Leclair, E. Kamionka, M.-L. Desrousseaux, H. Texier, S. Gavalda, M. Cot, E. Guémard, M. Dalibey, J. Nomme, G. Cioci, S. Barbe, M. Chateau, I. André, S. Duquesne, A. Marty, *Nature* 2020, 580, 7802, 216-219.

[10] Carbios, can be found under https://www.carbios.com/fr/. (accessed: 30 September 2024)

[11] G. Behrendt, B. W. Naber, *J. Univ. Chem. Technol. Metallurgy* **2009**, 44, 1, 3-23.

[12] L. Gausas, S. K. Kristensen, H. Sun, A. Ahrens, B. S. Donslund, A. T. Lindhardt, T. Skrydstrup, *JACS Au* **2021**, 1, 4, 517–524.

[13] a) T. Uekert, J. S. DesVeaux, A. Singh, S. R. Nicholson, P. Lamers, T. Ghosh, J. E. McGeehan, A. C. Carpenter, G. T. Beckham, *Green Chem.* **2022**, 24, 17, 6531-6543; b) L. Ritzen, B. Sprecher, C. Bakker, R. Balkenende, Resour. Conserv. Recycl. **2023**, 199, 107268; c) J. Liu, J. He, R. Xue, B. Xu, X. Qian, F. Xin, L. M. Blank, J. Zhou, R. Wei, W. Dong, M. Jiang, *Biotechnol Adv.* **2021**, 48, 107730; d) J. Datta, M. Włoch, in *Polyurethane Polymers: Blends and Interpenetrating Polymer Networks* (Eds.: S. Thomas, J. Datta, J. T. Haponiuk, A. Reghunadhan) Elsevier Inc., **2017**, pp. 323–358; e) D. Simón, A. M. Borreguero, A. de Lucas, J. F. Rodríguez, *Waste Manag.* **2018**, 76, 147-171; f) A. Kemona, M. Piotrowska, *Polymers* **2020**, 12, 8, 1752.

[14] a) N. Mahajan, P. Gupta, *RSC Adv.* **2015**, 5, 41839-41854; b) R. Nugraha Catur Utomo, Wing-Jin Li, Till Tiso, C. Eberlein, M. Doeker, H. J. Heipieper, A. Jupke, N. Wierckx, L. M. Blank, *ACS Sustainable Chem. Eng.* **2020**, 8, 47; 17466–17474; c) R. Wei, W. Zimmermann, *Microb. Biotechnol.* **2017**, 10, 6, 1308-1322; d) M. Orlando, G. Molla, P. Castellani, V. Pirillo, V. Torretta, N. Ferronato, *Int. J. Mol. Sci.* **2023**, *24*, 4, 3877; e) A. Magnin, E. Pollet, V. Phalip, L. Avérous, *Biotechnol. Adv.* **2020**, 39, 107457; f) J. Liu, J. He, R. Xue, B. Xu, X. Qian, F. Xin, L. M. Blank, J. Zhou, R. Wei, W. Dong, M. Jiang, *Biotechnol. Adv.* **2021**, 48, 107730; g) A. Raczyńska, A. Góra, I. André, *Biotechnol. Adv.* **2024**, 77, 108439.

[15] a) A. Magnin, L. Hoornaert, E. Pollet, S. Laurichesse, V. Phalip, L. Avérous, *Microb. Biotechnol.* 2019, 12, 3, 544-555; b) P. Bhavsar, M. Bhave, H. K. Webb, *World J. Microbiol. Biotechnol.* **2023**, 39, 122; c) A. Xu, J. Zhou, L. M. Blank, M. Jiang, *Trends Microbiol.* **2023**, 31, 7, 668-671; d) Y. Akutsu-Shigeno, Y. Adachi, C. Yamada, K. Toyoshima, N. Nomura, H. Uchiyama, T. Nakajima-Kambe, *Appl. Microbiol. Biotechnol* **2006**, 70, 4, 422–429; e) T. Nakajima-Kambe, F. Onuma, N. Kimpara, T. Nakahara, *FEMS Microbiol. Lett.* **1995**, 129, 1, 39-42; f) Y. H. Peng, Y. H. Shih, Y. C. Lai, Y. Z. Liu, Y. T. Liu, N. C. Lin, *Environ. Sci. Pollut. Res. Int.* **2014**, 21, 16; g) J. Liu, J. Liu, B. Xu, A. Xu, S. Cao, R. Wei, J. Zhou, M. Jiang, W. Dong, *Chemosphere* **2022**, 304, 135263.

[16] J. Schmidt, R. Wei, T. Oeser, L. A. Dedavid e Silva, D. Breite, A. Schulze, W. Zimmermann, *Polymers* **2017**, 9, 2.

[17] J. Álvarez-Barragán, L. Domínguez-Malfavón, M. Vargas-Suárez, R. González-Hernández, G. Aguilar-Osorio, and H. Loza-Tavera, *Appl, Environ Microbiol.* **2016**, 82, 17.

[18] A. Magnin, E. Pollet, L. Avérous, in *Methods in Enzymology*, *Vol. 648* (G. Weber, U. T. Bornscheuer, R. Wei) Academic Press Inc., **2021**, pp. 317–336.

[19] Y. Branson, S. Söltl, C. Buchmann, R. Wei, L. Schaffert, C. P. S. Badenhorst, L. Reisky, G. Jäger, U. T. Bornscheuer, *Angew. Chem. Int. Ed.* **2023**, 62, e202216220.

[20] T. Bayer, G. J. Palm, L. Berndt, H. Meinert, Y. Branson, L. Schmidt, C. Cziegler, I. Somvilla, C. Zurr, L. G. Graf, U. Janke, C. P. S. Badenhorst, S. König, M. Delcea, U. Garscha, R. Wei, M. Lammers, U. T. Bornscheuer, *Angew. Chem. Int. Ed.* **2024**, 63, e202404492.

[21] L. Cong, Z. S. Li, J. Gao, Q. Li, Y.Y. Chen, X. Han, W. Gert, R. Wei, W. D. Liu, U. T. Bornscheuer, 2024, Crystal structure of a novel PU plastic degradation urethanase UMG-SP2 from uncultured bacterium, PDB databank, doi.org/10.2210/pdb8WDW/pdb

[22] D. Ollis, E. Cheah, M. Cygler, B. Dijkstra, F. Frolow, S. Franken, M. Harel, S. Remington, I. Silman, J. Schrag, J. Sussman, K. Verschueren, A. Goldman, *Protein Eng.* **1992**, 5, 3.

[23] R. Kourist, H. Jochens, S. Bartsch, R. Kuipers, S. K. Padhi, M. Gall, D. Böttcher, H.-J. Joosten, U. T. Bornscheuer, *ChemBioChem* **2010**, 11, 1635-1643.

[24] H. Chebrou, F. Bigey, A. Arnaud, P. Galzy, *BBA* **1996**, 1298, 285-293.

[25] J. Labahn, S. Neumann, G. Büldt, M. R. Kula, J. Granzin, *J. Mol. Biol.* **2002**, 322, 5, 1053-1064.

[26] S. Shin, T.-H. Lee, N.-C. Ha, H. M. Koo, S.-y. Kim, H.-S. Lee, Y. S. Kim, B.-H. Oh, *EMBO J.* **2002**, 21, 11, 2509 - 2516.

[27] B.W. Weber, S. W. Kimani, A. Varsani, D.A. Cowan, R. Hunter, G.A. Venter, J.C. Gumbart, B.T. Sewell, *J Biol. Chem*. **2013**, 288, 40, 28514-28523.

[28] A. L. B. Valiña, D. Mazumder-Shivakumar, T. C. Bruice, *Biochem.* **2004**, 43, 50, 15657–15672.

[29] L. Holm, DaliLite v.5, Program for Structural Alignment, University of Helsinki, Helsinki (Finland), **2019**.

[30] C.-A. Min, J.-S. Yun, E. H. Choi, U. W. Hwang, D.-H. Cho, J.-H. Yoon, J. H. Chang, *Crystals* **2019**, 9, 472.

[31] P. Tripathi, J. J. Mousa, N. S. Guntaka, S. D. Bruner, *Acta Crystallogr. D Struct. Biol.* 2023, 79, 830-836.

[32] M. K. McKinney, B. E. Cravatt, *Annu. Rev. Biochem.* **2005**, 74, 411-432.

[33] S. Dider, J. Ji, Z. Zhao, L. Xie, *npj Syst. Biol. Appl.* **2016**, 2, 160223.

[34] Z. Wu, C. Liu, Z. Zhang, R. Zheng, Y. Zheng, *Biotechnol Adv.* **2020**, 43, 107574.

[36] R. McCoy Vernon, P. A. Chong, B. Tsang, T. H. Kim, A. Bah, P. Farber, H. Lin, J. D. Forman-Kay, eLife **2018**, 7, e31486.

[37] W. Kabsch, *Acta Crystallogr D Biol Crystallogr* **2010**, 66, 2.

[38] M. F. Incardona, G. P. Bourenkov, K. Levik, R. A. Pieritz, A. N. Popov, O. Svensson, EDNA, Program for online analysis of Crystal Data, **2009**.

[39] A. J. McCoy, R. W. Grosse-Kunstleve, P. D. Adams, M. D. Winn, L. C. Storoni, R. J. Read, Phaser, Program for phasing macromolecular crystal structure, University of Cambridge, Cambridge (England), **2007**.

[40] J. Jumper, R. Evans, A. Pritzel, T. Green, M. Figurnov, O. Ronneberger, K. Tunyasuvunakool, R. Bates, A. Žídek, A. Potapenko, A. Bridgland, C. Meyer, S. A. A. Kohl, A. J. Ballard, A. Cowie, B. Romera-Paredes, S. Nikolov, R. Jain, J. Adler, T. Back, S. Petersen, D. Reiman, E. Clancy, M. Zielinski, M. Steinegger, M. Pacholska, T. Berghammer, S. Bodenstein, D. Silver, O. Vinyals, A. W. Senior, K. Kavukcuoglu, P. Kohli, D. Hassabis, *Nat.* **2021** 596, 7873, 583-589.

[41] P. V. Afonine, R. W. Grosse-Kunstleve, N. Echols, J. J Headd, N. W. Moriarty, M. Mustyakimov, T. C. Terwilliger, A. Urzhumtsev, P. H. Zwart, P. D. Adams, phenix.refine, program for automated structure solution, Lawrence Berkeley National Laboratory, Berkeley, CA (USA) **2012**.

[42] P. Emsley, K. Cowtan, Coot, Program for model-building, University of York, York, (England), **2004**.

[43] V. B. Chen, W. B. Arendall, J. J. Headd, D. A. Keedy, R. M. Immormino, G. J. Kapral, L. W. Murray, J. S. Richardson, D. C. Richardson, MolProbity, Program for structure validation, Duke University, Durham (USA), **2009**.

[44] E. F. Pettersen, T. D. Goddard, C. C. Huang, G. S. Couch, D. M. Greenblatt, E. C. Meng, T. E. Ferrin, UCSF Chimera, Program for macromolecular structure visualization, University of California, San Francisco (California, USA), **2004**.

[45] L. Zheng, U. Baumann, J. L. Reymond, *Nucleic Acids Res*. **2004**, 32, 14.

[46] G. Martínez-Rosell, T. Giorgino, G. De Fabritiis, ProteinPrepare, Program for protein preparation for Molecular Dynamics Simulations, University Pompeu Fabra, Barcelona (Spain), **2017**.

[47] M. H. M. Olsson, C. R. Søndergaard, M. Rostkowski, J. H. Jensen, PROPKA3, Program for treating internal and surface residues in empirical pK_a, University of Copenhagen, Copenhagen (Denmark), **2011**.

[48] J. A. Maier, C. Martinez, K. Kasavajhala, L. Wickstrom, K. E. Hauser, C. Simmerling, ff14SB, Program for improving protein side chains and backbone parameters, Stony Brook University, Stony Brook (New York, USA), **2015**.

[49] D.A. Case, D.S. Cerutti, T.E. Cheatham, III, T.A. Darden, R.E. Duke, T.J. Giese, H. Gohlke, A.W. Goetz, D. Greene, N. Homeyer, S. Izadi, A. Kovalenko, T.S. Lee, S. LeGrand, P. Li, C. Lin, J. Liu, T. Luchko, R. Luo, D. Mermelstein, K.M. Merz, G. Monard, H. Nguyen, I. Omelyan, A. Onufriev, F. Pan, R. Qi, D.R. Roe, A. Roitberg, C. Sagui, C.L. Simmerling, W.M. Botello-Smith, J. Swails, R.C. Walker, J. Wang, R.M. Wolf, X. Wu, L. Xiao, D.M. York and P.A. Kollman, AMBER 2017, University of California, San Francisco (USA), **2017**.

[50] M. J. Frisch, G. W. Trucks, H. B. Schlegel, G. E. Scuseria, M. A. Robb, J. R. Cheeseman, G. Scalmani, V. Barone, G. A. Petersson, H. Nakatsuji, X. Li, M. Caricato, A. Marenich, J. Bloino, B. G. Janesko, R. Gomperts, B. Mennucci, H. P. Hratchian, J. V. Ortiz, A. F. Izmaylov, J. L. Sonnenberg, D. Williams-Young, F. Ding, F. Lipparini, F. Egidi, J. Goings, B. Peng, A. Petrone, T. Henderson, D. Ranasinghe, V. G. Zakrzewski, J. Gao, N. Rega, G. Zheng, W. Liang, M. Hada, M. Ehara, K. Toyota, R. Fukuda, J. Hasegawa, M. Ishida, T. Nakajima, Y. Honda, O. Kitao, H. Nakai, T. Vreven, K. Throssell, J. A. Montgomery, Jr., J. E. Peralta, F. Ogliaro, M. Bearpark, J. J. Heyd, E. Brothers, K. N. Kudin, V. N. Staroverov, T. Keith, R. Kobayashi, J. Normand, K. Raghavachari, A. Rendell, J. C. Burant, S. S. Iyengar, J. Tomasi, M. Cossi, J. M. Millam, M. Klene, C. Adamo, R. Cammi, J. W. Ochterski, R. L. Martin, K. Morokuma, O. Farkas, J. B. Foresman, and D. J. Fox, Gaussian 09, Gaussian, Inc., Wallingford (Connecticut, USA) **2009**.

[51] L. Schrödinger, W. DeLano, The PyMOL Molecular Graphics System, Version 3.0 Schrödinger, LLC, **2020**.

[52] M. J. Abraham, T. Murtola, R. Schulz, S. Páll, J. C. Smith, B. Hess, E. Li ndahl, *SoftwareX* **2015**, 19-25.

[53] P. S. Nagle, F. Rodriguez, A. Kahvedžić, S. J. Quinn, and I. Rozas, *J Med Chem* **2009**, 52, 22, 7113-7121.

10.1002/anie.202419535

Entry for the Table of Contents

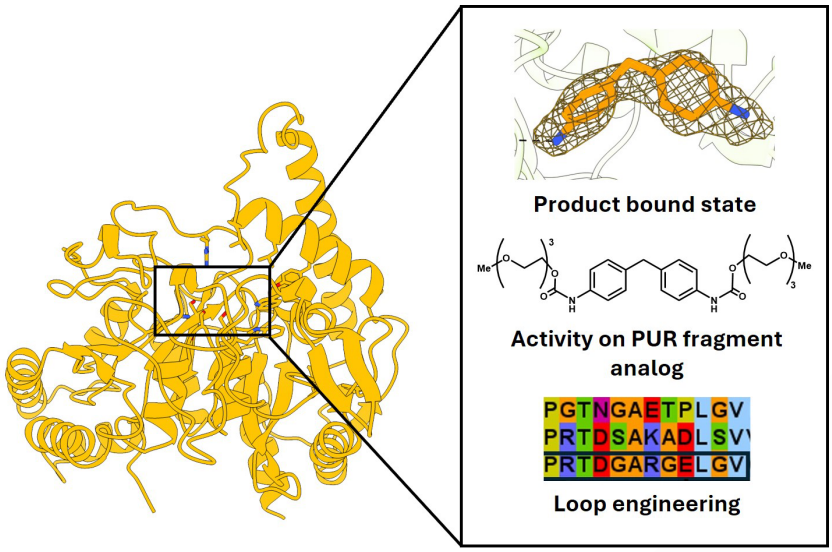

Global plastic production has surged in recent decades, leading to significant environmental waste. With a focus on polyurethane (PUR), the high-resolution crystal structure of the metagenomic urethanase SP3 in a product-bound state has been solved. Kinetic studies and enzyme engineering guided by the structure identified key structural elements that enhance urethanase activity, thereby supporting future PUR degradation and sustainable recycling efforts.